Batteries & Supercaps

Research Article
doi.org/10.1002/batt.202300093

Chemistry Europe
European Chemical Societies Publishing

www.batteries-supercaps.org

An Ether-Based Low Density Electrolyte for the Use of Graphite Anodes in Stable Lithium-Sulfur Batteries

Florian S. Hoffmann,[a, b] Florian Schmidt,[a, b] Jannes Müller,[c] Kay Schönherr,[b] Susanne Dörfler,[b] Thomas Abendroth,[b] Holger Althues,*[b] Arno Kwade,[c] Nae-Lih Wu,[d] and Stefan Kaskel[a, b]

Lithium sulfur (Li–S) batteries represent an interesting technology due to the high theoretical capacity of sulfur and the low cost of the cathode material. Li–S cells with graphite electrodes could be an option for low-cost stationary energy storage as graphite is cheap and the electrode production process is well established. Unfortunately, in most Li–S electrolytes, graphite is not stable due to solvent co-intercalation and degrades fast. In this work, a new low density electrolyte based on hexyl methyl ether (HME) and 1,3-dioxalane (DOL) is presented, which allows to use graphite as anode material for Li–S batteries. In symmetric graphite vs. graphite cells an averaged Coulombic efficiency of 99.94% per electrode could be reached. For the first time, cycling conditions like voltage window and balancing were optimized for Li–S cells with graphite anodes and the suitability of the concept could be demonstrated in multilayer pouch cells under realistic conditions.

Introduction

The rapid warming of our planet makes it essential to reduce emissions of greenhouse gases such as CO_2. Batteries are seen as playing a major role in this, as they can store regenerative energy and make it available for a wide range of applications. The sharp rise in demand for batteries (e.g., for electric cars) may lead to shortages of the metals lithium, nickel and cobalt in the next few years.[1] Due to that, substitution or better utilization of these elements is necessary.

An exciting next-generation battery in this context is the lithium-sulfur (Li–S) battery due to the high theoretical specific capacity of sulfur (1672 mAh g_S^{-1}) and the high abundance and therefore low cost of sulfur.[2] Thereby, Sulfur as cathode material could substitute the geopolitically, socially and environmentally problematic Co and Ni.[1]

Unfortunately, the state-of-the-art (SOTA) Li–S batteries still suffer problems like low cycle life, low Coulombic efficiency (CE) and fast self-discharge which hinder their broad commercialization.[3,4] These challenges are induced on the one hand by the so-called polysulfide shuttle and on the other hand by the instability of the lithium metal anode.[2,3]

During the conversion of sulfur to lithium sulfide, short and long chain polysulfides are formed, which can dissolve in the electrolyte and diffuse to the anode where they are reduced to Li_2S/Li_2S_2 and shorter-chain polysulfides.[5] These shorter-chain polysulfides could diffuse back to the cathode where they are reoxidized. In the last years, there were several efforts to overcome the polysulfide shuttle: carbons with tailored porosity,[6,7] doping carbons with hetero-atoms,[8] oxide additives,[9] coatings,[7,10] ion-selective separator[11] or specialized electrolytes.[12–14]

The other challenge is the instability of the lithium metal anode. The highly reactive lithium reacts with solvents, electrolyte salts and polysulfides, which leads to formation of a solid-electrolyte interface (SEI).[15] Due to the high volume change of the lithium anode during cycling, the SEI breaks open which exposes fresh lithium and leads to further electrolyte degradation and active material loss.[3,16,17] Another concern is the dendritic growth of lithium during deposition, which could cause safety issues.[17] To mitigate this obstacle, various approaches were developed such as new electrolytes,[18] electrolyte additives,[19] surface coatings[20] or the substitution of the anode material with silicon,[21,22] hard carbons[22,23] or graphite.[24–35]

Graphite is a very interesting anode material for Li–S batteries, as it has been the standard anode material of the lithium ion battery for decades and electrode production is

[a] Dr. F. S. Hoffmann, F. Schmidt, Prof. Dr. S. Kaskel
Department of Inorganic Chemistry
Technische Universität Dresden
Bergstraße 66, 01062 Dresden (Germany)
[b] Dr. F. S. Hoffmann, F. Schmidt, K. Schönherr, Dr. S. Dörfler, Dr. T. Abendroth, Dr. H. Althues, Prof. Dr. S. Kaskel
Business Unit Chemical Surface Technology
Fraunhofer IWS, Fraunhofer Institute for Material and Beam Technology (IWS)
Winterbergstraße 28, 01277 Dresden (Germany)
E-mail: holger.althues@iws.fraunhofer.de
[c] J. Müller, Prof. Dr. A. Kwade
Institute for Particle Technology, and Battery LabFactory Braunschweig (BLB)
Technische Universität Braunschweig
Volkmaroder Str. 5, 38104 Braunschweig (Germany)
[d] Prof. Dr. N.-L. Wu
Department of Chemical Engineering
National Taiwan University
Roosevelt Road, Sec. 4, No. 1, Taipei, 10617 (Taiwan)

Supporting information for this article is available on the WWW under https://doi.org/10.1002/batt.202300093

Research Article
doi.org/10.1002/batt.202300093
Chemistry Europe
European Chemical Societies Publishing

well established on industrial scale. For these reasons, there have also been some attempts to establish graphite in Li–S batteries over the last 15 years. However, graphite is not stable in standard ether based Li–S electrolytes due to intercalation of the solvent and exfoliation of the graphene layers. Hence, Li–S batteries do not work with carbonate based electrolytes due to the reaction of polysulfides with carbonate solvents.[28] Therefore, in order to successfully cycle the sulfur-graphite system anyway, the following concepts were developed: 1) confinement of the sulfur in special cathode structures and use of carbonate electrolytes;[35] 2) special binders for the anode material;[27] 3) special separators and the use of two separated electrolytes;[34] 4) use of ether electrolytes with high conducting salt concentrations (solvent-in-salt);[25,29–31] and 5) use of special solvents that strongly reduce the polysulfide solubility (sparingly solvating solvents).[26,28,32,33] Unfortunately, many publications only show characterization in coin cells and sometimes use thick separators, large amounts of electrolyte or low sulfur loadings. This makes a realistic evaluation of these concepts difficult.

In this work, various ether electrolytes with low polysulfide solubility are investigated for their compatibility with graphite. With the most promising electrolyte, the cycling conditions (voltage window, balancing) of the sulfur-graphite cells were then optimized and cells were evaluated under realistic conditions in pouch cells.

Results and Discussion

Electrolyte evaluation

Previous publications on lithium-sulfur cells with graphite anodes have used sparingly solvating electrolytes consisting of lithium bis(trifluoromethanesulfonyl)imide (LiTFSI), a well lithium-salt dissociating solvent like tetraglyme or sulfolane, and a fluorinated solvent which is hardly involved in solvation (sparingly solvating solvent) like 1,1,2,2-tetrafluoroethyl 2,2,3,3-tetrafluoropropyl ether (TTE) or bis(2,2,2-trifluoroethyl) ether (BTFE).[26,28,32,33] Unfortunately, these fluorinated ethers usually have a high density, which has a negative impact on specific energy of the battery.[13] A previous study by our group has shown good performance of hexyl methyl ether (HME) based electrolytes in lithium sulfur batteries at low electrolyte volumes.[13,36] HME effectively suppresses polysulfide solubility while having a low density of 0.776 g cm^{-3}.[37] Polysulfide solubility can be adjusted by adding limited amounts of 1,2-dimethoxyethane (DME) or 1,3-dioxolane (DOL) to the HME-based electrolytes to improve the kinetics of the Li–S battery.[13] Based on the experience from the previous study, we initially tested three HME based electrolytes in graphite half-cells (Figure 1a): 2 M LiTFSI in HME (density: 1.03 g cm^{-3}), 2 M LiTFSI in HME/DOL (9 : 1) (1.09 g cm^{-3}) and 2 M LiTFSI in HME/DME (8 : 2) (1.07 g cm^{-3}). The SOTA electrolyte of the Li–S battery 1 M LiTFSI in DME/DOL (1 : 1) + 0.5 M $LiNO_3$ (1.12 g cm^{-3}) was chosen as a reference.

The cell with the DME/DOL reference electrolyte shows an initial specific lithiation capacity of 507 mAh g_{Gr}^{-1} but only a specific delithiation capacity of 168 mAh g_{Gr}^{-1}. In the subsequent cycles, the capacity decreases rapidly. This lithiation capacity, which is higher than the theoretical capacity of graphite (372 mAh g_{Gr}^{-1}), suggests the occurrence of irreversible side reactions, such as electrolyte degradation or the intercalation of Li-solvent clusters. This is already known and was studied in previous publications.[31] In contrast, the cells with HME/DOL (9 : 1), HME/DME (8 : 2) and HME electrolyte show lithiation capacities of 390 mAh g_{Gr}^{-1}, 384 mAh g_{Gr}^{-1} and 387 mAh g_{Gr}^{-1}, and delithiation capacities of 362 mAh g_{Gr}^{-1}, 354 mAh g_{Gr}^{-1} and 359 mAh g_{Gr}^{-1}, respectively. The resulting initial Coulombic efficiencies (ICEs) of 92.8 %, 92.3 % and 92.7 % are comparable to the ICE of graphite in carbonate electrolytes like 1 M lithium hexafluorophosphate in dimethyl carbonate/ethylene carbonate (1 : 1).[38] The capacity loss can be explained by the formation of a solid electrolyte interface (SEI) on the graphite electrode.[38]

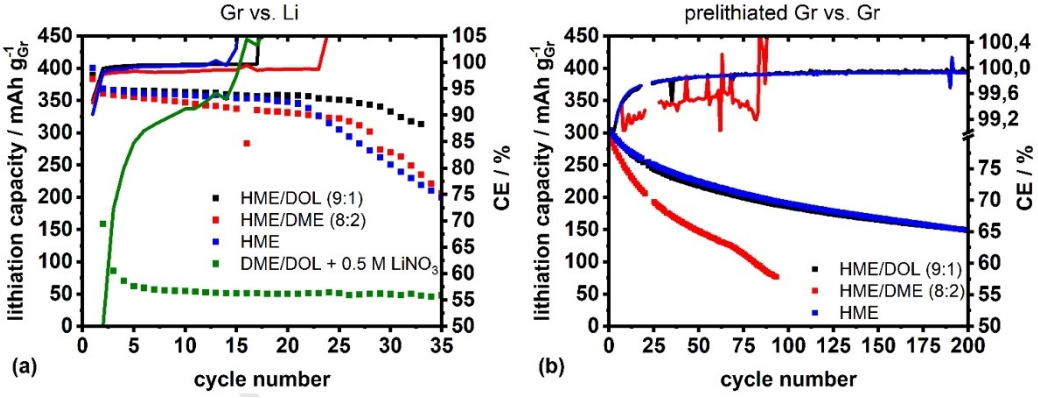

Figure 1. Galvanostatic cycling of a) graphite vs. lithium half-cells and b) symmetrical prelithiated graphite vs. graphite cells with different electrolytes: 2 M LiTFSI in HME/DOL (9 : 1), 2 M LiTFSI in HME/DME (8 : 2), 2 M LiTFSI in HME, 1 M LiTFSI in DME/DOL (1 : 1) + 0.5 M $LiNO_3$. The specific capacity of the symmetrical cells is based on the original weight of the prelithiated graphite electrode before prelithiation. Unfortunately, due to a technical problem, 5 cycles were not recorded by the battery tester for the symmetrical cells.

In the three HME based electrolytes, the specific lithiation capacity is stable for about 20–25 cycles at approx. 350 mAh g_{Gr}^{-1} before it continuously decreases. This drop is not necessarily caused by the degradation of the graphite electrode, but can also be caused by the drying out of the cell or the degradation of the lithium anode.

The voltage curves of the graphite half-cells (Figure S1) show a strong increase of the overpotential during lithiation and delithiation of the graphite, especially for the HME/DME and HME electrolyte. This indicates an increasing cell resistance during cycling. Due to the high reactivity of the lithium anode with the electrolyte, a SEI is formed on the anode. During cycling, the lithium anode exhibits a pronounced volume change and an irregular lithium deposition, which repeatedly destroys the SEI and thereby exposes fresh lithium. Due to the formation of a new and additional SEI on the fresh lithium, more electrolyte is consumed. Therefore, the interfacial resistance of the cell is rising as the thickness of SEI is growing and the electrolyte volume is depleting.

To exclude the influence of the lithium anode, symmetrical graphite vs. graphite cells were investigated (Figure 1b). This characterization was inspired by the work of Burns et al.[39] and thus it is possible to investigate the stability of the graphite electrodes and the parasitic side reactions independently from the cathode material or lithium metal. For this characterization, a graphite electrode is prelithiated in the half-cell setup and subsequently reassembled against a fresh electrode with the same geometry and loading. The same electrolyte was used for the prelithiation as later in the symmetrical cell. Figure 1(b) shows the lithiation capacity of the prelithiated graphite electrode during cycling, which is equivalent to the discharge capacity of an NCM/Gr full cell.

For the three electrolytes HME/DOL (9:1), HME/DME (8:2) and HME, delithiation capacities of 352 mAh g_{Gr}^{-1}, 328 mAh g_{Gr}^{-1} and 338 mAh g_{Gr}^{-1}, subsequent lithiation capacities of 314 mAh g_{Gr}^{-1}, 292 mAh g_{Gr}^{-1} and 304 mAh g_{Gr}^{-1} and ICE of 89.3%, 89.2% and 89.9% are achieved in the first cycle, respectively. The relatively high losses come from the formation of an SEI on the fresh graphite electrode. The symmetric cells with HME/DOL (9:1) and HME show relatively good stability with capacities of 149 mAh g_{Gr}^{-1} after 200 cycles. This is especially remarkable since there is no lithium reservoir in these cells and any loss will affect the capacity. The average CE between 4th and 200th cycle is also very high at 99.88% and 99.87%, respectively. It should be noted that there are two graphite electrodes in the cell. Thus, the average loss per electrode is half as large[39] and therefore the CE per electrode is approx. 99.94%. Only HME/DME (8:2) showed a relatively rapid drop in capacity and did not achieve 200 cycles. The average CE was also significantly lower, suggesting that DME co-intercalates in graphite or other parasitic side reactions occur. Co-intercalation of DME in graphite has also been observed in previous publications.[40]

Insights can also be gained from the voltage curves of the symmetrical cells. When cell resistances increase during cycling, the overpotential rises and a hysteresis is increasingly formed. To better represent this, the normalized capacities were depicted in Figure S2. For cells with HME/DOL and HME electrolyte, the overpotential increases mainly in the first cycles and then remains fairly constant. The overpotential increase in the first cycles can be explained by the formation of an SEI on the fresh graphite electrode and thus an increase of the interfacial resistance. In contrast, the cells with HME/DME show a continuously rising overpotential during cycling, which indicates an increase in cell resistance due to the continuous growth of the SEI, drying out of the cell due to electrolyte loss or clogging of the separator by degraded graphite particles or flakes.

To investigate the electrolytes further, Li–S cells with graphite anodes were characterized (Figure 2). As in the case of Gr vs. Gr cells, the graphite electrodes were electrochemically prelithiated for this purpose. These initial full cell experiments were not intended to optimize the cycle parameters, but to determine the basic suitability of the electrolytes. Therefore, a relatively low sulfur loading of approx. 1.4 $mg_S\,cm^{-2}$, an areal capacity ratio of the anode to the cathode (n/p-ratio) of 1.7:1 and a sulfur-to-electrolyte ratio (E/S-ratio) of 10 $\mu L\,mg_S^{-1}$ was chosen. A voltage window between 1.4 V and 2.5 V was selected for cycling. In a previous study of our group, the voltage window for Li–S cells with lithium anode and HME based electrolytes was optimized to 1.5–2.5 V. Graphite shows a discharge plateau at 0.1 V vs. Li/Li^+ (Figure S1). Due to the large overbalancing of the anode, the graphite is only be cycled in this plateau region, which is why the lower cut-off voltage is adjusted to 1.4 V. Since the potential of the fully lithiated graphite is 0.005 V vs. Li/Li^+, the upper termination voltage was not altered.

The results of the Li–S cells (Figure 2) confirm the results of the Gr vs. Gr cells that the performance of the graphite electrode with HME/DME (8:2) electrolyte is significantly worse than with HME/DOL (9:1) and HME electrolyte. Probably due to hindered wetting, the cell with HME/DME electrolyte showed low capacities in the first cycles. After the 4th cycle, the capacity stabilizes, but with 592 mAh g_S^{-1} it is still significantly lower

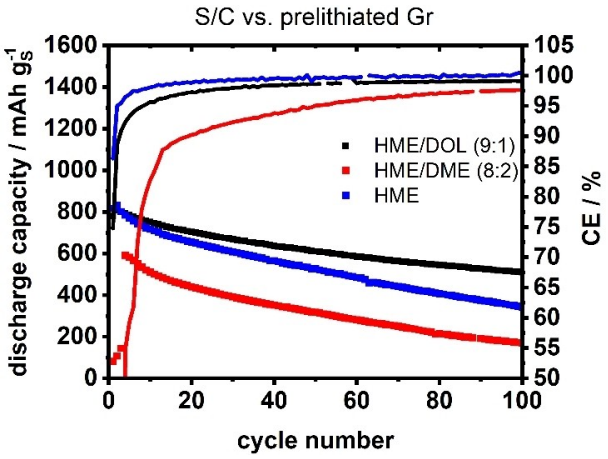

Figure 2. Galvanostatic cycling of Li–S full cells with prelithiated graphite anode using different electrolytes: 2 M LiTFSI in HME/DOL (9:1), 2 M LiTFSI in HME/DME (8:2), 2 M LiTFSI in HME.

than the capacity of the cells with HME/DOL and HME/DME electrolyte. In the 4th cycle, they reach capacities of 795 mAh g_S^{-1} and 784 mAh g_S^{-1}, respectively. When comparing the cells with HME/DOL and HME, the capacities are comparable at the beginning, but the cell with HME electrolyte demonstrates significantly faster degradation.

After 100 cycles, a discharge capacity of 510 mAh g_S^{-1} is achieved with HME/DOL, 341 mAh g_S^{-1} with HME and 170 mAh g_S^{-1} with HME/DME which corresponds to a capacity retention of 63%, 41% and 29%, respectively. For the cell with HME/DME, the discharge capacity of the 4th cycle was used instead of the 1st cycle to calculate the capacity retention.

In terms of CE, the cell with HME/DME also has a significantly lower CE in each cycle than the cells with the other two electrolytes. This indicates more pronounced side reactions or a stronger polysulfide shuttle. The polysulfide solubility, determined as sulfur concentration, is 0.45 M for the HME/DME and 0.40 M for the HME/DOL electrolyte.[13,36] Thus, the significantly lower CE of HME/DME compared to HME/DOL must be caused by side reactions other than the polysulfide shuttle. Considering the results of the Gr vs. Gr cells with HME/DME, side reactions of the electrolyte at the graphite anode are probably mainly responsible for the low CE.

Comparing the average CE of cells with HME/DOL and HME between 4th and 100th cycle, the CE of the cell with HME/DOL is slightly lower with 98.1% than that of the cell with HME with 99.4% (HME/DME with 92.7%). Considering the relatively similar results of the two electrolytes in the Gr vs. Gr cells, this difference can be attributed to a small polysulfide shuttle in HME/DOL. In HME, almost no polysulfides dissolve, suppressing the polysulfide shuttle almost completely. Nevertheless, the CE of cells with both electrolytes is good, especially compared to the SOTA electrolyte DME/DOL in Li–S cells with lithium metal anode.[14]

However, the barely existing polysulfide solubility in HME is also disadvantageous. The lack of solubility limits the electrochemical conversion of sulfur kinetically, provokes a deposition of an electrically insulating layer on the cathode material and pore blocking.[13] This results in loss of active material and increased cell resistance.[13] These effects could be the reasons for the slightly higher cell degradation of cells with HME compared to cells with HME/DOL.

In summary, the HME/DOL electrolyte is the best electrolyte for Li–S cells with graphite electrode among those tested and was therefore selected for further experiments.

Characterization of electrolyte-graphite-interaction

To further investigate the interaction of the graphite electrode with the HME/DOL (9:1) electrolyte, scanning electron microscopy (SEM, Figure 3) and X-ray diffraction (XRD, Figure 4) were performed on cyclized graphite electrodes. For this purpose, graphite electrodes were cycled against lithium in the half-cell setup for 10 cycles and then disassembled in the delithiated state. The electrodes were directly measured without further washing steps. As a reference, cells with SOTA DME/DOL electrolyte were examined. On the SEM images of the pristine graphite electrode (Figure 3a) cuboidal to spherical particles with diameters between 5–20 μm could be seen. The particles are relatively smooth and show few cracks or edges.

In the graphite electrodes which were cycled in DME/DOL (Figure 3b), the original particles are pulverized and many cracks and particle fragments are visible. As already known in the literature,[26] the use of DME/DOL electrolyte leads to co-intercalation of solvent-ion complexes and this results in exfoliation of the graphene layer. This exfoliation can lead to cracks and pulverization of the particles. In contrast, after cycling in HME/DOL, the graphite particles seem unchanged from the pristine state (Figure 3c).

XRD can also be used to evaluate whether the crystallinity of the graphite is preserved during cycling or reduced, for example, by exfoliation of the graphite. The stacking of the graphene layers in the graphite is characterized by a strong reflection at 26.5° (Laue indices 002) and a higher order diffraction at 54.6° (indices 004) (Figure 4). In the case of graphite which was cycled in DME/DOL, these two peaks disappear almost completely, confirming the exfoliation of the graphite. In contrast, both peaks remain in the cycled graphite from the cell with HME/DOL.

In summary, the results show the stability of graphite in HME/DOL and that no or hardly any delamination occurs due to co-intercalation of the solvent.

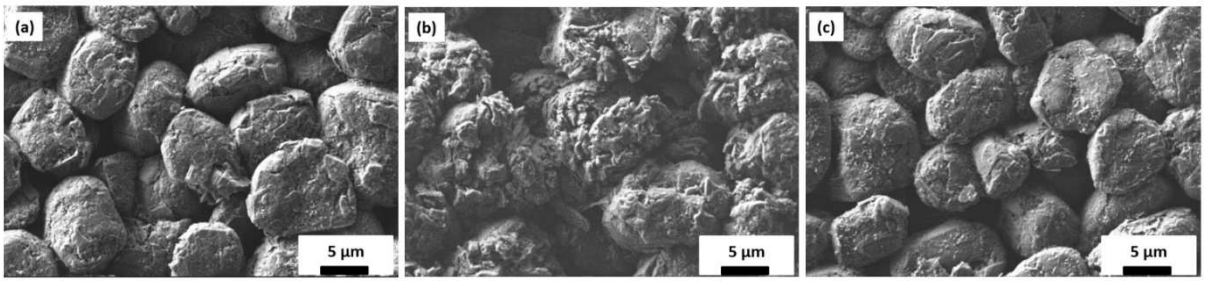

Figure 3. Scanning electron microscopy (SEM) images of graphite electrodes a) before cycling and after cycling in Gr vs. Li half-cells for 10 cycles using b) 1 M LiTFSI in DME/DOL (1:1) + 0.5 M $LiNO_3$ or c) 2 M LiTFSI in HME/DOL (9:1) as electrolyte.

Research Article
doi.org/10.1002/batt.202300093
Chemistry Europe
European Chemical Societies Publishing

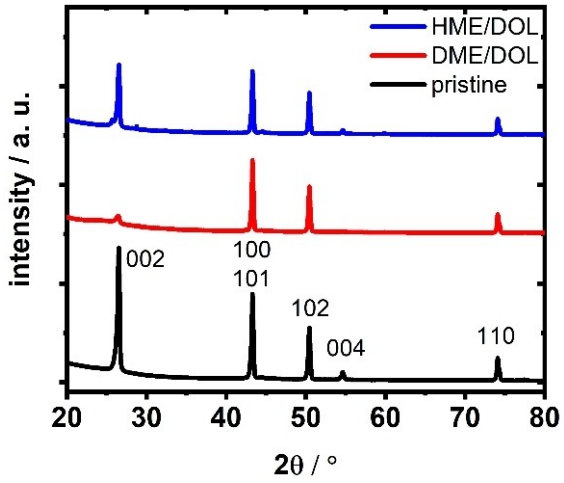

Figure 4. X-ray diffraction data of a pristine graphite electrode and post-mortem graphite at delithiated state which were cycled in Gr vs. Li half-cells for 10 cycles using 1 M LiTFSI in DME/DOL (1:1) + 0.5 M $LiNO_3$ or 2 M LiTFSI in HME/DOL (9:1) as electrolyte. The indexing was performed based on the work of Howe et al.[41]

Optimization of cell parameters

As in the first Li–S cells with HME/DOL electrolyte only approx. 800 mAh g_S^{-1} could be achieved in the initial cycle and the voltage curves (Figure S3) showed an unusual sloping range at the end of charging at voltages above 2.4 V, the voltage window as well as the capacity balancing of anode and cathode were reviewed. To analyze the voltage window, 3-electrode cells are best suited because the electrochemical potentials of the cathode and anode could be recorded separately. For this purpose, cells were assembled with S/C composite as cathode, prelithiated graphite as anode and metallic lithium as reference with HME/DOL as electrolyte and a n/p-ratio of 1.76:1. The potential curves of the cathode and anode against Li/Li^+ in the first cycle are shown in Figure 5(a).

Due to the overbalancing of the anode, it is not completely delithiated during the first discharge and shows a plateau-like behavior. However, contrary to the assumptions when defining the voltage window, this potential is not constant at 0.1 V vs. Li/Li^+ but 0.11 V at the beginning of discharge and 0.18 V at the end. Graphite also shows a relatively constant potential when the cell is charged: 0.10 V vs. Li/Li^+ at the beginning of charge and 0.09 V at the end. The fact that at the end of charging the graphite potential is not at 0.005 V vs. Li/Li^+ but higher, indicates that the graphite is not completely lithiated again as lithium ions were lost. The potential of graphite has a great influence on the potential curve of the cathode. Due to the plateau-like potential of the graphite, the basic potential curve of the cathode is similar to cells with lithium anode but the cut-off potentials are shifted. At the end of discharging, the cathode only reaches a potential of 1.58 V vs. Li/Li^+ in contrast to the targeted 1.5 V, which is why the cathode is not fully utilized and the specific capacity is reduced. At the end of charging, a potential of 2.58 V vs. Li/Li^+ is reached. Due to this high potential, additional side reactions can occur which have a negative impact on the performance of the cell. This could be the cause of the sloping section in the voltage curves of the Li–S full cells at the end of charging (Figure S3). To ensure full utilization of the cathode and at the same time minimize side reactions, the voltage window of the full cells should be adjusted to 1.3–2.4 V.

Observing the progression of the cut-off potentials during cycling is interesting as it allows us to better understand degradation processes in the cell (see Figure S4a). The cut-off potential of graphite at the end of discharge increases slightly in the first five cycles and then remains relatively constant at 0.22 V vs. Li/Li^+ until the 40th cycle. Also, the cut-off potential at the end of charging remains constant during cycling and decreases slightly from 0.09 V vs. Li/Li^+ in the second cycle to 0.08 V in the 40th cycle. This suggests that the capacity loss during cycling (Figure S4b) is not mainly caused by a loss of cyclable lithium ions, but by a loss of sulfur due to polysulfide shuttling or precipitation of large S_8 or Li_2S crystallites that cannot be readdressed. If the main reason of the capacity loss was lithium ion consumption, then at some point the lithium reservoir would have to be depleted and the graphite cut-off

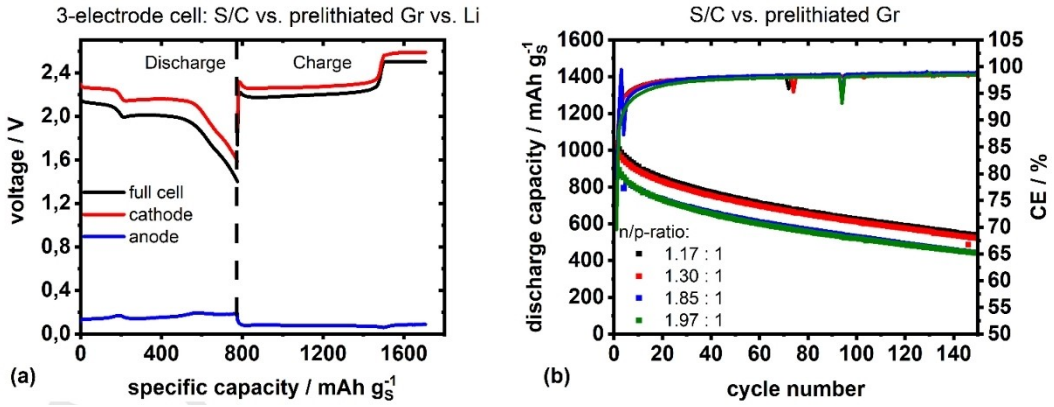

Figure 5. a) Voltage profiles of the 1st cycle of 3-electrode cells containing a S/C cathode, prelithiated graphite anode and Li as reference electrode with n/p-ratios of 1.76:1. 2 M LiTFSI in HME/DOL (9:1) was used as electrolyte. b) Galvanostatic cycling of Li–S full cells with prelithiated graphite anode using varying n/p-ratios. The n/p-ratio is the quotient of the areal capacity of the anode divided by the areal capacity of the cathode.

potential at the end of discharge should increase rapidly. Due to the constant cut-off potential of the graphite, the cut-off potentials of the cathode also remain constant.

The rapid drop in capacity in the 3-electrode cell compared to the coin cells is caused by the design of the 3-electrode cell. A thick glass fiber separator (1.55 mm thick) is required to attach the lithium reference electrode securely at the side. Further, a high electrolyte volume of 350 µL is required to wet them completely. This corresponds to an electrolyte/sulfur ratio of 135 $\mu L\,mg_S^{-1}$ which leads to an increased dissolution of polysulfides. Furthermore, polysulfides can adsorb to the glass fiber separator, resulting in further losses of active material. Unfortunately, the authors are not aware of a simple 3-electrode setup under realistic conditions (low electrolyte amount, thin separator), so this should be explored separately in further studies.

The balancing of the negative to the positive electrode has a great influence on, among others, the specific capacity, CE and potential curves which has been shown by Kasnatscheew et al., our group and others in previous publications for lithium-ion cathodes with graphite[42] or silicon[43] anodes. Therefore, to determine the best balancing, Li–S full cells with n/p-ratios between 1.17:1 and 1.97:1 were assembled and characterized in the optimized voltage window between 1.3 V and 2.4 V (Figure 5b). Therefore, the areal capacity of the graphite anodes was kept as constant as possible for all cells and the loading of the S/C composites was varied. HME/DOL (9:1) was chosen as electrolyte and the total electrolyte amount was set to 35 µL so that cathode, anode and separator are completely wetted with electrolyte. This results in a slight variation of the E/S-ratio between approx. 10 $\mu L\,mg_S^{-1}$ and 15 $\mu L\,mg_S^{-1}$.

During the first discharge of the Li–S cell (lithiation of sulfur), there is a linear dependency of the specific capacity on the n/p-ratio: For n/p-ratios 1.17:1, 1.30:1, 1.85:1, 1.97:1, the specific capacities are 960 $mAh\,g_S^{-1}$, 943 $mAh\,g_S^{-1}$, 833 $mAh\,g_S^{-1}$ and 814 $mAh\,g_S^{-1}$. Also, the initial CE decreases from 80.8% (n/p-ratio 1.17:1) to 69.5% (1.97:1). Some characteristics like higher lithium reservoir, higher E/S-ratio and lower total current (current is calculated based on S content) at higher n/p-ratio, would suggest an increasing specific capacity. The decreasing specific capacity is probably due to passivation reactions of the graphite anode. Although the electrodes have been prelithiated and thus a stable SEI should be established, small amounts of polysulfides can still react with the polarized surface of the graphite. Since all cells have the same surface area of graphite, but a lower total amount of sulfur with increasing n/p-ratio, these passivation reactions lead to higher relative losses.

Also, the capacity retention (Figure S5) after 150 cycles decreases slightly with increasing n/p-ratio from 53.3% at 1.17:1 to 49.4% at 1.97:1. Thereby, the quantity of lithium is not the limiting factor in lithium-sulfur cells with graphite anode. In this case, the cell with the lowest n/p ratio would have to have the lowest cycling stability or capacity retention.

Summarizing, the Li–S cell with a balancing of 1.17:1 shows the best performance and this balancing was used for further experiments.

Integration of next-generation materials

Compared to other anode materials, graphite has the disadvantage of a relatively low theoretical specific capacity of 372 $mAh\,g^{-1}$. Thus, numerous attempts were made in recent years to increase this capacity while at the same time maintaining stability. An interesting approach is the addition of 5–20% silicon nanoparticles, with silicon increasing the capacity and graphite buffering the large volume variations of the silicon during lithiation and delithiation.[44]

In a previous publication,[44] scientists of TU Braunschweig and National Taiwan University developed an innovative process to fabricate these Gr/Si composites and coated the composite with carbon, which could further enhance the electrochemical performance. The composite shows a specific capacity of 600 $mAh\,g^{-1}$, which is approximately two times higher than that of pure graphite. This electrode was electrochemically prelithiated like the graphite electrodes and then assembled against an S/C cathode with an n/p-ratio of 1.15:1 and cycled in the voltage window between 1.3 V and 2.4 V (Figure 6a).

The initial discharge capacity of the cell with Gr/Si composite is slightly lower with 906 $mAh\,g_S^{-1}$ than the one based on commercial graphite (Gr) with 960 $mAh\,g_S^{-1}$. Also, the capacity retention with 52.2% after 100 cycles and the average CE between 4th and 100th cycle with 95.5% is slightly lower as for graphite with 62.1% and 97.7% respectively. Presumably, the graphite matrix and carbon coating failed to completely buffer the volume change of the silicon and thus prevent the SEI from breaking up. Nevertheless, these results are very promising, since the anode mass could be reduced by 40% while only a slight capacity deterioration was observed.

Pouch cell characterization

To validate the performance of this promising concept, it must be scaled up and evaluated under realistic conditions in large-scale demonstrator cells. Therefore, multilayer Li–S pouch cells (approx. 0.5 Ah) with graphite and Gr/Si composite anodes were assembled. Therefore, five-layer half-cells (Gr/Li/Gr/Li/Gr) were first assembled and the graphite or Gr/Si anodes were electrochemically prelithiated in a similar way to the coin cells. Subsequently, the cells were disassembled and the electrodes were directly assembled against S/C cathodes without washing. Unfortunately, there were problems disassembling the commercial graphite electrodes in pouch cell format. Therefore, in-house fabricated graphite electrodes (Gr-2) were evaluated instead. The n/p ratio was set to 1.15:1 and the voltage window was adjusted to 1.3–2.4 V. A Li–S cell with lithium metal anode was also tested as a reference. The same n/p ratio was set, which is why the lithium anode had a layer thickness of approximately 20–21 µm. Since it is very cost-intensive to produce such thin lithium layers with the conventional rolling process, a melt coating process developed at Fraunhofer IWS[45] was used to produce the lithium layers.

Research Article
doi.org/10.1002/batt.202300093
Chemistry Europe
European Chemical Societies Publishing

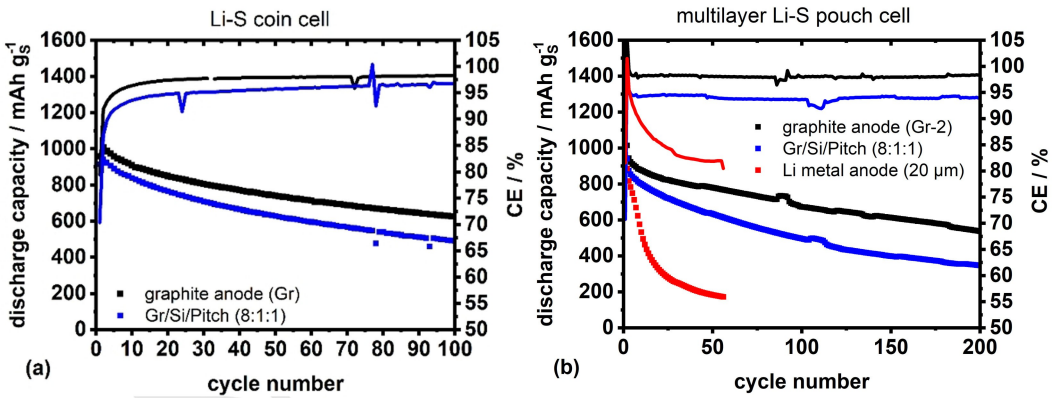

Figure 6. a) Galvanostatic cycling of Li–S coin cells with prelithiated silicon/graphite composite anode with carbon coating and with prelithiated commercial graphite as reference. b) Galvanostatic cycling of multilayer Li–S pouch cells with prelithiated graphite, prelithiated Gr/Si composite or lithium metal anode with similar areal capacity (20 µm thickness). 2 M LiTFSI in HME/DOL (9:1) was used as electrolyte and the n/p-ratio was set to 1.15:1.

The results of the electrochemical tests are illustrated in Figure 6(b). All cells achieve a specific discharge capacity of approx. 1000 mAh g_S^{-1} in the first cycle and thus the values are comparable to the results of the coin cells. However, while the cells with graphite (Gr-2) and Gr/Si composite anodes can be cycled for over 200 cycles, the cell with metallic lithium anode degrades fast and the specific discharge capacity decreases below 200 mAh g_S^{-1} within 50 cycles. This shows the great advantage of the concept using graphite based anodes. While cells with metallic lithium are no longer stable with a low lithium excess of 15%, the ones with graphite anodes are. Most studies on Li–S cells with metallic lithium anode in the literature use lithium excesses of more than 300%.

Comparing graphite and Gr/Si, cells with graphite again show slightly higher stability. After 100 cycles, cells with graphite achieve a capacity retention of 66.3% and 52.8% after 200 cycles. Meanwhile, with Gr/Si it is only 52.8% and 36.9%, respectively. The retention values are thus again comparable to the coin cell results, although the pouch cells with in-house-made graphite anodes (Gr-2) are slightly more stable than the coin cells with commercial graphite (Gr). An interesting effect is observed for the CE. While the CE of the coin cells increases continuously in the first few cycles and approaches values of approx. 98% for cells with graphite and 96% for cells with Gr/Si, the CE of pouch cells is constant from the third cycle and hardly changes. In pouch cells the average CE between 3rd and 200th cycle is 98.0% for cells with graphite and 93.9% with Gr/Si.

This work demonstrates the general feasibility of S/C vs. Graphite and S/C vs. Graphite/Si cells based on ether electrolytes. With further improvement of cycling stability this can be a concept for low cost energy storage in future.

Conclusions

In summary, the suitability of a low density electrolyte based on hexyl methyl ether (HME) and 1,3-dioxalane (DOL) for stable cycling of graphite in Li–S cells without special cathodes or separators was demonstrated. Li–S cells with graphite electrodes are an interesting option for low-cost stationary energy storage due to their high stability at low lithium excesses. Until now, only electrolytes with high salt concentrations or fluoroethers could guarantee stable performance of graphite anodes without special cathodes or separators. However, these concepts are expensive and the high density of the electrolyte lowers the energy density of the cells significantly. The stability of graphite in the new electrolyte was demonstrated in symmetric graphite vs. graphite cells with stable cycling over 200 cycles and an average CE of 99.94% per electrode. The interaction between electrolyte and graphite was studied by XRD and SEM. After 10 cycles, no significant changes in the morphology of the graphite particles (SEM) were observed and their crystallinity was preserved as well. This demonstrates suppressed co-intercalation of the solvents which would lead to exfoliation of the graphite. Furthermore, for the first time experiments were conducted to optimize the cycling conditions of Li–S full cells with graphite anode. In order to make best use of the Li–S cathode, these were characterized in 3-electrode cells with graphite anode and lithium reference electrode and the voltage window was adjusted based on the results. The influence of balancing was also investigated and it was demonstrated that a relatively low overbalancing of the anode shows the best results, since only small amounts of sulfur are then lost through side reactions with graphite. The Li–S cells with graphite anodes and newly developed electrolyte could be successfully scaled up into multilayer pouch cells and showed a satisfying performance over 200 cycles (capacity retention of 52.8%) with a limited lithium excess of only 15%. The reference cell containing a lithium metal anode with the same lithium excess degraded remarkably faster and retained less than 200 mAh g_S^{-1} after 50 cycles. It was also possible to demonstrate possible further developments of the concept by partially substituting graphite with silicon which could improve the specific energy and energy density of the system.

Research Article
doi.org/10.1002/batt.202300093

Experimental Section

Electrode preparation

Ketjenblack EC600JD (KB, Nouryon Specialty Chemicals B.V.) was mixed with sulfur (Sigma Aldrich, Inc., $\geq$ 99.5 %) in a weight ratio of 1:2 and heated under air at 155 °C for 0.5 h (melt-infiltration process). Afterwards, the S/C composites were mixed with multi-walled carbon nanotubes (MWCNT, Nanocyl 7000, Nanocyl SA.) and poly(tetrafluoroethylene) (PTFE) in a weight ratio of 90:7:3 and then processed into electrodes in the solvent-free DRYtraec® process.[46] Finally, they were transferred on a primer coated aluminium current collector (thickness 18 μm). The composition of the final electrodes is S/KB/MWCNT/PTFE in the ratio 60:30:7:3. These cathodes were developed, evaluated, and discussed in previous publications.[47] Two batches of electrodes were made to perform the balancing experiments: The first batch with a sulfur loading of (1.40 ± 0.10) mg cm^{-2} and a density of (0.35 ± 0.03) g cm^{-3} and the second batch with a loading of (2.20 ± 0.15) mg cm^{-2} and a density of (0.48 ± 0.04) g cm^{-3}. Considering a theoretical specific capacity of 1672 mAh g^{-1}, the loadings correspond to approximately 2.3 mAh cm^{-2} and 3.7 mAh cm^{-2}, respectively.

The commercial graphite (Gr) electrodes consist of natural graphite and were purchased from Custom Cells Itzehoe GmbH. These were used for all coin cell tests. The active material content was 96 %, the electrode density was 1.3 g cm^{-3} and a 14 μm thick blank copper foil was used as current collector. Electrodes with mass loadings of (6.90 ± 0.65) mg cm^{-2} and (12.70 ± 0.75) mg cm^{-2} were used corresponding to areal capacities of approximately 2.4 mAh cm^{-2} and 4.4 mAh cm^{-2}, respectively (specific capacity of 350 mAh g^{-1}).

The production of the silicon/graphite (Gr/Si) composite electrodes with pitch coating is described in an earlier publication.[44] The composite consisted of 80 % graphite, 10 % silicon nano-particles (PyroPowders GmbH) and 10 % pitch coating (pitch from China Steel Corp.). This composite was coated with carboxymethyl cellulose (Dow Chemical)/styrene-butadiene rubber (Zeon Corp.) (CMC/SBR, 2:1) as binder and Super C65 as conductive additive (Imerys Graphite and Carbon S.A.) on 10 μm thick dendritic copper foil (Furukawa Electric Co., Ltd.). The composite/binder/conductive additive ratio was 90:5.4:4.6. The mass loading of the Gr/Si composite was (4.6 ± 0.1) mg cm^{-2} for the coin cell tests and (6.7 ± 0.1) mg cm^{-2} for the pouch cell tests which corresponds to areal capacities of approx. 2.8 mAh cm^{-2} and 4.0 mAh cm^{-2}, respectively.

Prelithiation of the commercial graphite anodes for the pouch cell tests resulted in delamination of the coating during disassembly, so another graphite electrodes (Gr-2) were produced in-house using the same process as for the Si/Gr electrodes. These Gr-2 electrodes had a graphite/binder/conductive additive ratio of 90:5.4:4.6, a graphite mass loading of (11.5 ± 0.1) mg cm^{-2} and an areal loading of approx. 4.3 mAh cm^{-2}. The electrodes were coated on 10 μm thick dendritic copper foil (Furukawa Electric Co., Ltd.).

The reference lithium metal films for the pouch cell tests were produced using a melt deposition process developed at Fraunhofer IWS.[45] First, a 12 μm thick Cu foil (Schlenk Metallfolien GmbH & Co. KG) was pretreated in a roll-to-roll furnace (HTM Reetz) at 300 °C for 180 s to form a lithiophilic CuO layer. This film was double-side coated with liquid lithium (purity: 99.95 %, Cellithium) in an argon-filled glovebox (M. Braun Inertgas-Systeme GmbH, H_2O and O_2 < 0.01 ppm) through a homemade apparatus, keeping the lithium bath at a temperature of 210 °C. The substrate velocity during coating was 1.5 m min^{-1}. The resulting electrodes have lithium thicknesses of approx. 20–21 μm.

Electrolyte preparation

Electrolyte preparation was performed in an argon filled glovebox (M. Braun Inertgas-Systeme GmbH, H_2O and O_2 < 0.01 ppm). Hexyl methyl ether (HME, TCI Deutschland GmbH), 1,2-dimethoxyethane (DME, Gotion Inc.) and 1,3-dioxolane (DOL, Gotion Inc.) were dried three times over molecular sieve (3 Å, Sigma Aldrich Inc.) before usage. Lithium bis(trifluoromethanesulfonyl)imide (LiTFSI, Gotion Inc.) and partially $LiNO_3$ (Alfa Aesar) were added to the different solvents and the electrolytes were stirred overnight. The indicated salt concentration refers to the volume of the solvents without considering excess volume due to mixing.

Electrochemical characterization

All test cells were assembled in an argon filled glovebox (M. Braun Inertgas-Systeme GmbH, H_2O and O_2 < 0.01 ppm) and characterized by a BaSyTec CTS test system (BaSyTec GmbH). All tests were performed at least as double determinations.

Coin cell measurements

The Gr vs. Li half-cell tests, symmetrical Gr vs. Gr tests and S/C vs. Gr coin cells were performed in CR2016 cell cases.

For the half-cell tests, a commercial graphite electrode (Gr, diameter: 16 mm) was assembled against a lithium chip (diameter: 16.5 mm, thickness: 250 μm, purity: 99.9 %, Xiamen Tmax Battery Equipments Limited) with a PE based separator (thickness 12 μm), 40 μL electrolyte and a 1000 μm thick stainless steel spacer (Fraunhofer IWS). The cells were cycled in a voltage window between 0.005 V and 1.5 V with a C-rate of C/10 (1 C = 350 mA g_{Gr}^{-1}) and constant voltage steps (CVS) at the end of charge and discharge until C/100.

For the Gr vs. Gr and S/C vs. Gr coin cells, a prelithiated graphite electrode is needed what was done electrochemically. The cells were assembled identically to the half-cells and cycled three times in the same voltage window with C-rate of C/20 (CVS until C/100) and then the graphite was prelithiated with C/20 (CVS until C/100) to a voltage of 0.005 V. The coin cells were then opened in an argon filled glovebox and the graphite electrode was integrated directly into the new cell.

The prelithiated graphite electrode (diameter 16 mm) was assembled against a fresh graphite electrode with the same diameter, a 12 μm thick PE separator, 40 μL electrolyte and a 1000 μm thick stainless steel spacer. A voltage window between −1.0 V and 1.0 V was chosen. After a formation cycle with C/20 (CVS until C/100), the cells were cycled with C/10 (CVS until C/100).

The S/C vs. Gr cells were assembled using S/C electrodes (diameter: 15 μm), similar prelithiated graphite electrodes, separator and spacer. For the electrolyte evaluation and the cells with Si/Gr composite, the sulfur loading was approx. 2.2 mg$_S$ cm^{-2} and the electrolyte amount was calculated based on an electrolyte/sulfur ratio (E/S-ratio) of 10 μL mg$_S^{-1}$. For the balancing evaluation (sulfur loading between 1.4 mg$_S$ cm^{-2} and 2.2 mg$_S$ cm^{-2}), the electrolyte amount was set to 35 μL which resulted in E/S-ratios between 10 μL mg$_S^{-1}$ and 15 μL mg$_S^{-1}$. The areal capacity ratios of the anode and cathode (n/p-ratio) were determined based on the theoretical specific sulfur capacity of the cathode and the practical lithiation capacity of the graphite electrode in the prelithiation cell. In the beginning, the voltage window was set to 1.4–2.5 V. Considering the results of the 3-electrode cells, the voltage window was then changed to 1.3–2.4 V to best utilize the cathode. After a formation cycle with C/20 (1 C = 1672 mA g$_S^{-1}$) in charge and discharge, the

cell was cycled with C/20 on charge and C/10 on discharge. In the formation cycle and the further cycles, the charging contained a CVS until C/100.

3-electrode measurements

The 3-electrode experiments were performed in ECC-Ref cells (EL-Cell GmbH) containing a S/C cathode (diameter: 15 mm), a prelithiated graphite electrode (preparation see paragraph above, diameter: 16 mm), a glass fiber separator (thickness 1.55 mm, EL-Cell GmbH) and 350 µL electrolyte. The thick separator is needed for implementation of the metallic lithium (purity: 99.9%, Xiamen Tmax Battery Equipments Limited) as reference electrode. The cells were tested with the same test procedure as for the coin cell testing.

Pouch cell measurements

Prelithiated graphite anodes or Gr/Si anodes were required for the Li–S pouch cells. Therefore, one double-sided and two single-sided Gr-2 or Gr/Si electrodes with dimensions of 71 mm × 46 mm were assembled against two metallic lithium electrodes (2 × 50 µm Li, China Energy Lithium Co., Ltd.) with the same dimensions together with 12 µm thick PE separators and 3.5 mL electrolyte. The prelithiation test plan was the same as for the coin cells. Subsequently, the cells were disassembled and the prelithiated electrodes were directly assembled against two double-sided S/C cathodes (sulfur loading approx. 2.2 $mg_S cm^{-2}$, dimensions 71 mm × 46 mm). PE separators of 12 µm thickness were also used for the Li–S cells, the amount of electrolyte was adjusted to an E/S-ratio of 10 $\mu L\, mg_S^{-1}$ and the n/p-ratio was 1.15 : 1. The cells were tested in a voltage window of 1.3–2.4 V with the same test plan as in coin cells. The reference cells with the melt-coated lithium anodes had the same electrode dimensions, n/p-ratio, separator and electrolyte amount. Also, the test plan was similar. Only the voltage window was set to 1.5–2.5 V.

Scanning electron microscopy (SEM)

The images were taken using a scanning electron microscope JSM-6610LV (JEOL GmbH) with detection of secondary electrons. For the *post-mortem* characterization, the cells were assembled in the Gr vs. Li setup and cycled for 10 cycles. Afterwards, the cells were opened in an argon filled glovebox and the electrodes were directly transferred to the microscope chamber.

X-ray diffraction (XRD) measurements

XRD measurements were performed on the diffractometer D5005 (Siemens AG) in the Bragg–Brentano arrangement. Cu-$K_{\alpha 1}$ radiation (wavelength 0.15405 nm) was used and measured in an angular range $10° < 2\theta < 80°$. The step size of each measurement point was 0.05° per step with a measurement time of 0.2 s each. The diffractograms shown were averaged from about 230 individual measurements.

Acknowledgements

This work has received funding from the Federal Ministry of Education and Research, Germany (BMBF), in the project LiBest (03XP0133B, 03XP0133D) and LiBest2 (03XP0304B, 03XP0304C) and from the National Science and Technology Council (NSTC) in Taiwan (NSTC 111-2923-E-011-001). The authors thank Jeannette Strangalies for performing the SEM measurements. Open Access funding enabled and organized by Projekt DEAL.

Conflict of Interests

The authors declare no conflict of interest.

Data Availability Statement

The data that support the findings of this study are available from the corresponding author upon reasonable request.

Keywords: 3-electrode measurement · capacity balancing · energy conversions · intercalations · pouch cell characterization

[1] C. Xu, Q. Dai, L. Gaines, M. Hu, A. Tukker, B. Steubing, *Commun. Mater.* **2020**, *1*, 437.
[2] A. Manthiram, S.-H. Chung, C. Zu, *Adv. Mater.* **2015**, *27*, 1980.
[3] R. Cao, W. Xu, D. Lv, J. Xiao, J.-G. Zhang, *Adv. Energy Mater.* **2015**, *5*, 1402273.
[4] Y. V. Mikhaylik, J. R. Akridge, *J. Electrochem. Soc.* **2004**, *151*, A1969–A1976.
[5] a) L. Borchardt, M. Oschatz, S. Kaskel, *Chem. Eur. J.* **2016**, *22*, 7324; b) M. Wild, L. O'Neill, T. Zhang, R. Purkayastha, G. Minton, M. Marinescu, G. J. Offer, *Energy Environ. Sci.* **2015**, *8*, 3477; c) C. Barchasz, F. Molton, C. Duboc, J.-C. Leprêtre, S. Patoux, F. Alloin, *Anal. Chem.* **2012**, *84*, 3973.
[6] a) F. Hippauf, W. Nickel, G.-P. Hao, K. Schwedtmann, L. Giebeler, S. Oswald, L. Borchardt, S. Doerfler, J. J. Weigand, S. Kaskel, *Adv. Mater. Interfaces* **2016**, *3*, 1600508; b) C. Kensy, D. Leistenschneider, S. Wang, H. Tanaka, S. Dörfler, K. Kaneko, S. Kaskel, *Batteries & Supercaps* **2021**, *4*, 612; c) P. Strubel, S. Thieme, T. Biemelt, A. Helmer, M. Oschatz, J. Brückner, H. Althues, S. Kaskel, *Adv. Funct. Mater.* **2015**, *25*, 287; d) S. Xin, L. Gu, N.-H. Zhao, Y.-X. Yin, L.-J. Zhou, Y.-G. Guo, L.-J. Wan, *J. Am. Chem. Soc.* **2012**, *134*, 18510; e) F. Böttger-Hiller, P. Kempe, G. Cox, A. Panchenko, N. Janssen, A. Petzold, T. Thurn-Albrecht, L. Borchardt, M. Rose, S. Kaskel et al., *Angew. Chem. Int. Ed. Engl.* **2013**, *52*, 6088; f) G. He, S. Evers, X. Liang, M. Cuisinier, A. Garsuch, L. F. Nazar, *ACS Nano* **2013**, *7*, 10920.
[7] X. Ji, K. T. Lee, L. F. Nazar, *Nat. Mater.* **2009**, *8*, 500.
[8] a) S. Dörfler, P. Strubel, T. Jaumann, E. Troschke, F. Hippauf, C. Kensy, A. Schökel, H. Althues, L. Giebeler, S. Oswald et al., *Nano Energy* **2018**, *54*, 116; b) C. Kensy, P. Härtel, J. Maschita, S. Dörfler, B. Schumm, T. Abendroth, H. Althues, B. V. Lotsch, S. Kaskel, *Carbon* **2020**, *161*, 190; c) H.-J. Peng, T.-Z. Hou, Q. Zhang, J.-Q. Huang, X.-B. Cheng, M.-Q. Guo, Z. Yuan, L.-Y. He, F. Wei, *Adv. Mater. Interfaces* **2014**, *1*, 1400227; d) C. Schneidermann, C. Kensy, P. Otto, S. Oswald, L. Giebeler, D. Leistenschneider, S. Grätz, S. Dörfler, S. Kaskel, L. Borchardt, *ChemSusChem* **2019**, *12*, 310; e) F. Sun, J. Wang, H. Chen, W. Li, W. Qiao, D. Long, L. Ling, *ACS Appl. Mater. Interfaces* **2013**, *5*, 5630; f) C.-P. Yang, Y.-X. Yin, H. Ye, K.-C. Jiang, J. Zhang, Y.-G. Guo, *ACS Appl. Mater. Interfaces* **2014**, *6*, 8789.
[9] a) C. J. Hart, M. Cuisinier, X. Liang, D. Kundu, A. Garsuch, L. F. Nazar, *Chem. Commun.* **2015**, *51*, 2308; b) X. Ji, S. Evers, R. Black, L. F. Nazar, *Nat. Commun.* **2011**, *2*, 325; c) X. Liang, C. Y. Kwok, F. Lodi-Marzano, Q. Pang, M. Cuisinier, H. Huang, C. J. Hart, D. Houtarde, K. Kaup, H. Sommer et al., *Adv. Energy Mater.* **2016**, *6*, 1501636; d) M.-S. Song, S.-C. Han, H.-S. Kim, J.-H. Kim, K.-T. Kim, Y.-M. Kang, H.-J. Ahn, S. X. Dou, J.-Y. Lee, *J. Electrochem. Soc.* **2004**, *151*, A791–A795.
[10] a) K. T. Lee, R. Black, T. Yim, X. Ji, L. F. Nazar, *Adv. Energy Mater.* **2012**, *2*, 1490; b) Y. Li, L. Yuan, Z. Li, Y. Qi, C. Wu, J. Liu, Y. Huang, *RSC Adv.* **2015**, *5*, 44160; c) S. Thieme, M. Oschatz, W. Nickel, J. Brückner, J. Kaspar, H. Althues, S. Kaskel, *Energy Technol.* **2015**, *3*, 1007; d) C. Wang, W. Wan, J.-T. Chen, H.-H. Zhou, X.-X. Zhang, L.-X. Yuan, Y.-H. Huang, *J. Mater. Chem. A* **2013**, *1*, 1716; e) F. Wu, J. Chen, L. Li, T. Zhao, R. Chen, *J. Phys. Chem. C* **2011**, *115*, 24411.

[11] a) I. Bauer, S. Thieme, J. Brückner, H. Althues, S. Kaskel, *J. Power Sources* **2014**, *251*, 417; b) Z. Jin, K. Xie, X. Hong, Z. Hu, X. Liu, *J. Power Sources* **2012**, *218*, 163; c) T.-Z. Zhuang, J.-Q. Huang, H.-J. Peng, L.-Y. He, X.-B. Cheng, C.-M. Chen, Q. Zhang, *Small* **2016**, *12*, 381.
[12] a) N. Azimi, W. Weng, C. Takoudis, Z. Zhang, *Electrochem. Commun.* **2013**, *37*, 96; b) L. Cheng, L. A. Curtiss, K. R. Zavadil, A. A. Gewirth, Y. Shao, K. G. Gallagher, *ACS Energy Lett.* **2016**, *1*, 503; c) M. Cuisinier, P.-E. Cabelguen, B. D. Adams, A. Garsuch, M. Balasubramanian, L. F. Nazar, *Energy Environ. Sci.* **2014**, *7*, 2697; d) K. Dokko, N. Tachikawa, K. Yamauchi, M. Tsuchiya, A. Yamazaki, E. Takashima, J.-W. Park, K. Ueno, S. Seki, N. Serizawa et al., *J. Electrochem. Soc.* **2013**, *160*, A1304–A1310; e) L. Suo, Y.-S. Hu, H. Li, M. Armand, L. Chen, *Nat. Commun.* **2013**, *4*, 1481.
[13] C. Weller, J. Pampel, S. Dörfler, H. Althues, S. Kaskel, *Energy Technol.* **2019**, *7*, 1900625.
[14] C. Weller, S. Thieme, P. Härtel, H. Althues, S. Kaskel, *J. Electrochem. Soc.* **2017**, *164*, A3766–A3771.
[15] D. Aurbach, E. Pollak, R. Elazari, G. Salitra, C. Scordilis-Kelley, J. Affinito, *J. Electrochem. Soc.* **2009**, *156*, A694–A702.
[16] a) D. Aurbach, *J. Power Sources* **2000**, *89*, 206; b) D. Aurbach, E. Zinigrad, Y. Cohen, H. Teller, *Solid State Ionics* **2002**, *148*, 405; c) S. Xiong, K. Xie, Y. Diao, X. Hong, *J. Power Sources* **2013**, *236*, 181.
[17] X.-B. Cheng, R. Zhang, C.-Z. Zhao, Q. Zhang, *Chem. Rev.* **2017**, *117*, 10403.
[18] a) W. Xu, J. Wang, F. Ding, X. Chen, E. Nasybulin, Y. Zhang, J.-G. Zhang, *Energy Environ. Sci.* **2014**, *7*, 513; b) Reza Younesi, Gabriel M. Veith, Patrik Johansson, Kristina Edström, Tejs Vegge, *Energy Environ. Sci.* **2015**, *8*, 1905; c) M. Amereller, T. Schedlbauer, D. Moosbauer, C. Schreiner, C. Stock, F. Wudy, S. Zugmann, H. Hammer, A. Maurer, R. M. Gschwind et al., *Prog. Solid State Chem.* **2014**, *42*,39; d) M. D. Tikekar, S. Choudhury, Z. Tu, L. A. Archer, *Nat. Energy* **2016**, *1*, 1126.
[19] a) Y.-C. Hsieh, M. Leißing, S. Nowak, B.-J. Hwang, M. Winter, G. Brunklaus, *Cell Rep. Phys. Sci.* **2020**, *1*,100139; b) F. S. Reuter, C.-J. Huang, Y.-C. Hsieh, S. Dörfler, G. Brunklaus, H. Althues, M. Winter, S. D. Lin, B.-J. Hwang, S. Kaskel, *Batteries & Supercaps* **2021**, *4*, 347; c) H. Zhang, G. G. Eshetu, X. Judez, C. Li, L. M. Rodriguez-Martínez, M. Armand, *Angew. Chem. Int. Ed. Engl.* **2018**, *57*, 15002; d) N. Azimi, Z. Xue, L. Hu, C. Takoudis, S. Zhang, Z. Zhang, *Electrochim. Acta* **2015**, *154*, 205; e) Q. Q. Liu, L. Ma, C. Y. Du, J. R. Dahn, *Electrochim. Acta* **2018**, *263*, 237; f) Q. Pang, X. Liang, A. Shyamsunder, L. F. Nazar, *Joule* **2017**, *1*, 871.
[20] a) X. Liang, Q. Pang, I. R. Kochetkov, M. S. Sempere, H. Huang, X. Sun, L. F. Nazar, *Nat. Energy* **2017**, *2*, 17119; b) D. Lin, Y. Liu, W. Chen, G. Zhou, K. Liu, B. Dunn, Y. Cui, *Nano Lett.* **2017**, *17*, 3731; c) Y. Lu, S. Gu, X. Hong, K. Rui, X. Huang, J. Jin, C. Chen, J. Yang, Z. Wen, *Energy Storage Mater.* **2018**, *11*, 16; d) C. Yan, X.-B. Cheng, Y.-X. Yao, X. Shen, B.-Q. Li, W.-J. Li, R. Zhang, J.-Q. Huang, H. Li, Q. Zhang, *Adv. Mater.* **2018**, *30*, 1804461; e) D. Wang, W. Zhang, W. Zheng, X. Cui, T. Rojo, Q. Zhang, *Adv. Sci.* **2017**, *4*, 1600168; f) Y. Zhao, Y. Ye, F. Wu, Y. Li, L. Li, R. Chen, *Adv. Mater.* **2019**, *31*, e1806532.
[21] a) A. Baasner, S. Dörfler, M. Piwko, S. Desilani, J. Brückner, H. Althues, S. Kaskel, *J. Mater. Chem. A* **2018**, *6*, 14787; b) R. Elazari, G. Salitra, G. Gershinsky, A. Garsuch, A. Panchenko, D. Aurbach, *Electrochem. Commun.* **2012**, *14*, 21; c) M. Piwko, T. Kuntze, S. Winkler, S. Straach, P. Härtel, H. Althues, S. Kaskel, *J. Power Sources* **2017**, *351*, 183; d) M. Piwko, S. Thieme, C. Weller, H. Althues, S. Kaskel, *J. Power Sources* **2017**, *362*, 349; e) Y. Yang, M. T. McDowell, A. Jackson, J. J. Cha, S. S. Hong, Y. Cui, *Nano Lett.* **2010**, *10*, 1486.
[22] K. Hancock, J. Becherer, M. Hagen, M. Joos, M. Abert, D. Müller, P. Fanz, S. Straach, J. Tübke, *J. Electrochem. Soc.* **2018**, *165*, A6091–A6106.
[23] a) S. A. Ahad, R. Pitchai, A. M. Beyene, S. H. Joo, D. K. Kim, H.-W. Lee, *ChemSusChem* **2018**, *11*, 3402; b) J. Brückner, S. Thieme, F. Böttger-Hiller, I. Bauer, H. T. Grossmann, P. Strubel, H. Althues, S. Spange, S. Kaskel, *Adv. Funct. Mater.* **2014**, *24*, 1284; c) D. T. Nguyen, A. Hoefling, M. Yee, G. T. H. Nguyen, P. Theato, Y. J. Lee, S.-W. Song, *ChemSusChem* **2019**, *12*, 480; d) S. Thieme, J. Brückner, A. Meier, I. Bauer, K. Gruber, J. Kaspar, A. Helmer, H. Althues, M. Schmuck, S. Kaskel, *J. Mater. Chem. A* **2015**, *3*, 3808.
[24] a) M. Agostini, B. Scrosati, J. Hassoun, *Adv. Energy Mater.* **2015**, *5*, 1500481; b) X. He, J. Ren, L. Wang, W. Pu, C. Wan, C. Jiang, *ECS Trans.* **2006**, *2*, 47.
[25] A. Bhargav, M. Wu, Y. Fu, *J. Electrochem. Soc.* **2016**, *163*, A1543–A1549.
[26] S. Chen, Z. Yu, M. L. Gordin, R. Yi, J. Song, D. Wang, *ACS Appl. Mater. Interfaces* **2017**, *9*, 6959.
[27] F. Jeschull, D. Brandell, K. Edström, M. J. Lacey, *Chem. Commun.* **2015**, *51*, 17100.
[28] Z. Li, S. Zhang, S. Terada, X. Ma, K. Ikeda, Y. Kamei, C. Zhang, K. Dokko, M. Watanabe, *ACS Appl. Mater. Interfaces* **2016**, *8*, 16053.
[29] D. Lu, J. Tao, P. Yan, W. A. Henderson, Q. Li, Y. Shao, M. L. Helm, O. Borodin, G. L. Graff, B. Polzin et al., *Nano Lett.* **2017**, *17*, 1602.
[30] D. Lv, P. Yan, Y. Shao, Q. Li, S. Ferrara, H. Pan, G. L. Graff, B. Polzin, C. Wang, J.-G. Zhang et al., *Chem. Commun.* **2015**, *51*, 13454.
[31] J. Ming, Z. Cao, W. Wahyudi, M. Li, P. Kumar, Y. Wu, J.-Y. Hwang, M. N. Hedhili, L. Cavallo, Y.-K. Sun et al., *ACS Energy Lett.* **2018**, *3*, 335.
[32] T. Seita, Y. Matsumae, J. Liu, R. Tatara, K. Ueno, K. Dokko, M. Watanabe, *ACS Energy Lett.* **2020**, *5*, 1.
[33] H. Moon, T. Mandai, R. Tatara, K. Ueno, A. Yamazaki, K. Yoshida, S. Seki, K. Dokko, M. Watanabe, *J. Phys. Chem. C* **2015**, *119*, 3957.
[34] L. Wang, Y. Wang, Y. Xia, *Energy Environ. Sci.* **2015**, *8*, 1551.
[35] S. Zheng, Y. Chen, Y. Xu, F. Yi, Y. Zhu, Y. Liu, J. Yang, C. Wang, *ACS Nano* **2013**, *7*, 10995.
[36] T. Boenke, S. Kirchhoff, F. S. Reuter, F. Schmidt, C. Weller, S. Dörfler, K. Schwedtmann, P. Härtel, T. Abendroth, H. Althues, et al., *Nano Res.* **2022**.
[37] M. Frenkel, X. Hong, R. C. Wilhoit, K. R. Hall, in *Landolt-Börnstein - Group IV Physical Chemistry* (Hrsg.: K. R. Hall, K. N. Marsh), Springer-Verlag, Berlin/Heidelberg, **2001**, S. 339–368.
[38] J. Asenbauer, T. Eisenmann, M. Kuenzel, A. Kazzazi, Z. Chen, D. Bresser, *Sustain. Energy Fuels* **2020**, *4*, 5387.
[39] J. C. Burns, L. J. Krause, D.-B. Le, L. D. Jensen, A. J. Smith, D. Xiong, J. R. Dahn, *J. Electrochem. Soc.* **2011**, *158*, A1417–A1422.
[40] a) S. Maruyama, T. Fukutsuka, K. Miyazaki, T. Abe, *J. Appl. Electrochem.* **2019**, *49*, 639; b) M. C. Smart, B. V. Ratnakumar, S. Surampudi, Y. Wang, X. Zhang, S. G. Greenbaum, A. Hightower, C. C. Ahn, B. Fultz, *J. Electrochem. Soc.* **1999**, *146*, 3963.
[41] J. Y. Howe, C. J. Rawn, L. E. Jones, H. Ow, *Powder Diffr.* **2003**, *18*, 150.
[42] a) J. Kasnatscheew, T. Placke, B. Streipert, S. Rothermel, R. Wagner, P. Meister, I. C. Laskovic, M. Winter, *J. Electrochem. Soc.* **2017**, *164*, A2479–A2486; b) C.-S. Kim, K. M. Jeong, K. Kim, C.-W. Yi, *Electrochim. Acta* **2015**, *155*, 431; c) B. Son, M.-H. Ryou, J. Choi, S.-H. Kim, J. M. Ko, Y. M. Lee, *J. Power Sources* **2013**, *243*, 641.
[43] a) F. Reuter, A. Baasner, J. Pampel, M. Piwko, S. Dörfler, H. Althues, S. Kaskel, *J. Electrochem. Soc.* **2019**, *166*, A3265–A3271; b) A. Baasner, F. Reuter, M. Seidel, A. Krause, E. Pflug, P. Härtel, S. Dörfler, T. Abendroth, H. Althues, S. Kaskel, *J. Electrochem. Soc.* **2020**, *167*, 20516.
[44] J. Müller, M. Abdollahifar, A. Vinograd, M. Nöske, C. Nowak, S.-J. Chang, T. Placke, W. Haselrieder, M. Winter, A. Kwade et al., *Chem. Eng. J.* **2020**, *407*,126603.
[45] K. Schönherr, B. Schumm, F. Hippauf, R. Lissy, H. Althues, C. Leyens, S. Kaskel, *Chem. Eng. J. Adv.* **2022**, *9*, 100218.
[46] H. Althues, S. Tschöcke, B. Schumm, S. Kaskel, C. Schult, D. Fritsche, K. Schönherr, WO2018210723 A1, **2018**.
[47] a) F. Schmidt, S. Ehrling, K. Schönherr, S. Dörfler, T. Abendroth, H. Althues, S. Kaskel, *Energy Technol.* **2022**, *10*, 2100721; b) F. Schmidt, S. Kirchhoff, K. Jägle, A. De, S. Ehrling, P. Härtel, S. Dörfler, T. Abendroth, B. Schumm, H. Althues et al., *ChemSusChem* **2022**, *15*, e202201320.

Manuscript received: March 9, 2023
Revised manuscript received: April 20, 2023
Accepted manuscript online: April 25, 2023
Version of record online: May 9, 2023